Investigation Of The Reference Korean Man Radiography Using Different Build Up Factor Models

Abdulrahman A. Alfuraih
Department of Radiological Sciences, College of Applied Medical Science,
King Saud University,P.O. Box 10219, Riyadh 11433,Saudi Arabia, alfuraih@ksu.edu.sa

Abstract
In order to quantify the scattered photon beam during X-ray radiography, deterministic particle transport algorithm uses the buildup factor (BUF) and the primary beam. However, from existing models describing such parameter for multilayer attenuators, we investigated three commonly used ones (Lin & Jiang, Kalos and Burke & Beck). Thus, the High Definition Reference Korean man (HDRK) was exposed to 150keV photon point source and particle histories were computed comprising the attenuation of the primary beam and the scattered beam contribution. For that purpose, we developed an in-house C++ based program to store projected phantom images, at an imaging detector distant with 1m far from the source, with possible choice between concerned BUF models. The thorax part only of the HDRK man was irradiated and based on specific Geometric Progression (GP) fitting parameters, Compton and total attenuation coefficients and equivalent atomic number of 25 organs, computations were carried out. We found a close image similarity for both models of Lin & Jiang and Kalos (SSIM=0.94). Also, the projected image resolution was ordered in the following way from better to worst: Lin & Jiang, Kalos and Burke & Beck. A correct model choice will be of great interest to the large community of radiation physicists, in general, and to medical imaging, teletherapy and brachytherapy physicists, in particular, since multilayer BUF parameters are the key parameter for point kernel calculations..

Keywords:
Buildup Factor; Multilayer; Human Tissues ; Radiography; HDRK man

1.Introduction

In contemporary medical education, radiology plays a unique role in integrating science and medicine [1]. No other medical specialty regularly interacts with such a wide range of medical disciplines. The practice of neurology, neurosurgery, otolaryngology, cardiology, pulmonology, urology, gastroenterology, orthopedic surgery and a host of other pediatric and surgical specialties would be virtually impossible without the regular presence of diagnostic imaging [2].

From the many existing computational tools used for imaging process selection, we cite the point-kernel method [3-5] and the Monte Carlo simulation technique [6-11]. In terms of particle transport handling, the major difference between the two techniques is that one takes a microscopically-oriented approach to solving the problem, whereas the other takes a macroscopically-ori-

ented approach. By assuming beam-like propagation, the point-kernel (PK) technique gains time for decision-making. In addition to the important parameters that form a PK core, we also quantify the scattering contribution to the unscattered beam during particle-matter interactions via the buildup factor (BUF). As well as Monte Carlo simulation programs such as EGS4 [12] and Geant4 [13,14], many existing tools have been used for BUF computations, like PALLAS [15] and ASFIT [16]. Moreover, from the many modeling of BUF such as the Invariant embedding method [17,18], the Moments method [19], the Iterative method [20], we found the more sophisticated one called Geometric Progression (GP) fitting method [21]. Additionally, for GP fitting, we noted the one provided by Kalos [22] and by Burke and Beck [23] for monodirectional parallel-plane beams and stratified shields and the more recent one by Lin & Jiang [24] for isotropic point sources. However, all materials with high density and atomic number were not studied, especially for human tissues (since they assumed water medium to approximate most of them). On the other hand, there is increasing use of deterministic models in practical research and clinical applications, including ray-tracing methods and analytical models [25-26]. They have fewer computational problems compared to Monte Carlo (MC) technique and can deal with statistics correctly, so that fast simulations of transmission images are possible. By using deterministic methods, it is possible to treat photon scattering and reflection in medical imaging [27-28].

The main goal of this work is to develop a point-kernel method able provide projected image of the High Definition Reference Korean (HDRK) man phantom [29] irradiated with a photon point source. As part of the study, the ray-tracing method, combined with exposure dose buildup, was applied to the simulation of a radiographic image. Different buildup factor models were analyzed in terms of their effect on the image quality. Although our study was limited to monochromatic photon point source, our present work can be thought of as building on the attention already given by radiation physicists, especially in relation to point kernel-based preparation of treatment plans and diagnosis imaging of tumors.

2.Materials and Methods

Here, we will briefly describe the proposed parameterization models for BUF calculation of monolayer and multilayer attenuators followed by the C++ developed program for the needed computations. Finally, we will describe the followed image analysis.

2.1. BUF parameterization models

According to the GP fitting method, the BUF for monolayers can be written in the following form [21]:

$$\frac{B(X)-1}{b-1}=\begin{cases}\dfrac{K^X-1}{K-1}, if\ K\neq 1\\ X, if\ K=1\end{cases} \qquad (1)$$

where b = BUF(1) ± 5% and the depth X is expressed in mean free paths: 1mfp=1/($\mu\times\rho$) , with μ and ρ correspond to the linear attenuation coefficient and the atom-

ic density, respectively.

For $X \leq 40\ mfp$:

$$K = c \times X^a + d \times \frac{\tanh((X/X_k) - 2)) - \tanh(-2)}{1 - \tanh(-2)} \quad (2)$$

where, a, b, c, d and Xk are the five fitting parameters.

Meanwhile, the general BUF formula for multilayers can be written in the following form:

$$B\left(\sum_{i=1}^{n-1} X_i, X_n\right) = B_n(X_n) + \left[B_n\left(\sum_{i=1}^{n} X_i\right) - B_n(X_n)\right] \times \boldsymbol{K} \times C_n \quad (3)$$

with the geometric progression parameter:

$$\boldsymbol{K} = \frac{\mathrm{B}(\sum_{\mathrm{i}=1}^{\mathrm{n}-2} \mathrm{X_i}, \mathrm{X_{n-1}}) - 1}{\mathrm{B_n}(\sum_{\mathrm{i}=1}^{\mathrm{n}-1} \mathrm{X_i}) - 1} \quad (4)$$

where X1, X2, ..., Xn the thickness of n consecutive material forming the multi-layered shield, B_n ($\sum_{i=I}^{n} X^i$) and B_n (X_n) correspond to the BUF of the n^{th} layer for the overall and the last layers, respectively. The correction parameter, C_n, has many general forms. It depends on the arrangement of consecutive materials, especially in terms of equivalent atomic number *Zeq* (for each material it depends on the photon energy). From existing theories, we will study three commonly used models:

1.Kalos [22]:

1.

$$C_n = \begin{cases} 1.0, HZ/LZ \\ e^{-1.7X_n} + (\gamma\beta/K)(1 - e^{-X_n}), LZ/HZ \end{cases} \quad (5)$$

2. Burke & Beck [23]:

$$C_n = \begin{cases} e^{-X_n/\gamma} + 1.5(1 - e^{-X_n}), HZ/LZ \\ e^{-\gamma X_n} + (\gamma\beta/K)(1 - e^{-X_n}), LZ/HZ \end{cases} \quad (6)$$

3. Lin & Jiang [24]:

$$C_n = \begin{cases} \mathrm{e}^{(-1.08\beta \mathrm{X_n})} + 1.13\beta\ell(X_n), HZ/LZ \\ (\gamma/K)e^{-X_n} + 0.8\ell(X_n), LZ/HZ \end{cases} \quad (7)$$

with

$$\gamma = \frac{(\mu_C/\rho)_{n-1}}{(\mu_C/\rho)_n} \quad (8)$$

$$\beta = \frac{(\mu_t/\rho)_{n-1}}{(\mu_C/\rho)_n} \quad (9)$$

and

$$\ell(X_n) = \frac{\mathrm{B_n(X_n)+1}}{\mathrm{B_{n-1}(X_n)+1}}(1 - \mathrm{e^{-X_n}}) \quad (10)$$

where, *HZ/LZ* means the arrangement of medium with high *Zeq* followed by medium with low *Zeq* and μ_C/ρ and μ_t/ρ are the Compton and the total mass attenuation coefficients

Table 1. Exposure GP fitting coefficient (a, b, c, d and Xk) and equivalent atomic number for studied organs and 150keV photon source energy

Mat ID	Zeq	a	b	c	d	X_k
Adipose tissue	6.486	-0.227	4.173	2.657	0.1	14.125
Adrenal	7.424	-0.189	3.929	2.284	0.081	14.273
Bladder	7.731	-0.175	3.901	2.167	0.072	14.385
Blood	7.795	-0.172	3.895	2.144	0.07	14.408
Bone	11.534	-0.084	3.104	1.509	0.019	14.911
breast	6.486	-0.227	4.173	2.657	0.1	14.125
Colon	7.507	-0.185	3.921	2.252	0.078	14.304
ET	7.424	-0.189	3.929	2.284	0.081	14.273
Esophagus	7.424	-0.189	3.929	2.284	0.081	14.273
Gall bladder	7.424	-0.189	3.929	2.284	0.081	14.273
Heart wall	7.628	-0.179	3.91	2.206	0.075	14.348

Mat ID	Zeq	a	b	c	d	X_k
Kidney	7.66	-0.178	3.907	2.194	0.074	14.36
Liver	7.69	-0.177	3.905	2.183	0.073	14.371
Lung	7.721	-0.175	3.902	2.171	0.072	14.382
Muscle	7.673	-0.177	3.906	2.189	0.073	14.364
Oral mucosa	7.413	-0.189	3.93	2.288	0.081	14.269
Pancreas	7.505	-0.185	3.922	2.253	0.078	14.303
RBM	7.282	-0.195	3.942	2.339	0.085	14.22
salivary glands	7.328	-0.193	3.938	2.321	0.084	14.237
Skin	7.397	-0.19	3.932	2.294	0.082	14.263
Small intestine	7.507	-0.185	3.921	2.252	0.078	14.304
Spleen	7.69	-0.177	3.905	2.183	0.073	14.371
Stomach	7.507	-0.185	3.921	2.252	0.078	14.304
Thymus	7.424	-0.189	3.929	2.284	0.081	14.273
Thyroid	8.702	-0.145	3.696	1.939	0.054	14.541

2.2.Computation procedure

An in-house C++ program has been developed for computation purposes. The program inputs are the five GP coefficient and the Zeq arrays corresponding to 25 tissues and organs of the thorax irradiated zone of the HDRK phantom, as tabulated in Table 1. Also, μ_C/ρ and μ_t/ρ attenuation coefficients extracted from NIST website [30] and atomic density from literature [29], arrays have been included.

The photon irradiated zone, with point source located at 1m far from the imaging detector, as shown in Figure 1, correspond to 247×141×250 voxels of size 1.981×1.981× 2.0854 mm3. The photon energy was 150 keV and the detector plane has the dimensions of 700×700 mm2 and pixilated into 1×1 mm2. After reading the HDRK data, we have the possibility to choose the BUF parameterization model. During the computation we calculate the travelled distance between the point source and the detector pixel and determine the number layers (from 250 planes) with same material and the corresponding distance for each one. The program output has been saved into ascii file, which will be converted into image.

Fig. 1. Schematic view of the computational geometry setup

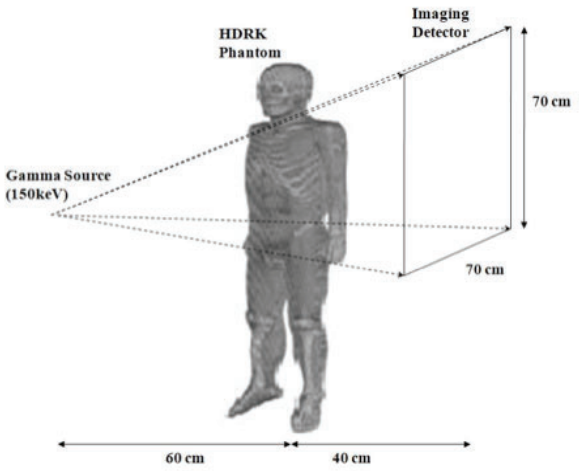

2.3. Statistical analysis

We used the Fiji [31] to read ascii output data of the developed program. Thanks to SNR [32] and SSIM [33] plugins, we are able to compare images in terms of signal-to-noise ratio (SNR), peak of signal-to-noise

ratio (PSNR), root mean square error (RMSE), mean average error (MAE) and structural similarity index (SSIM).

3.Results and Discussion

Figure 2 shows the projected image of the phantom without taking into account BUF. Moreover, such image results only from the exponential attenuation of the gamma ray along its trajectory from the source to the detector. We only see the overall shape of the phantom leading to a difficult interpretation of the image.

Fig. 2. Projected phantom image without taking into account for BUF parameter (BUF=1)

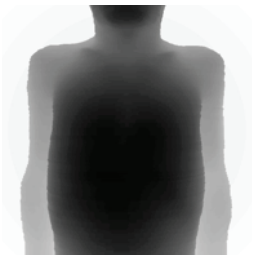

Fig. 3. Projected phantom image with BUF consideration for three models: Lin & Jiang (L&J), Burke & Beck (B&B) and Kalos (Kalos)

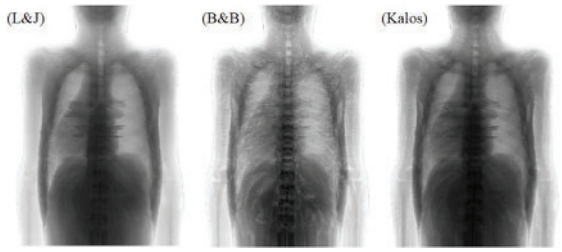

However, when we consider the BUF, describing the scattered flux contribution, the image becomes more interpretable and realistic, as shown in Figure 3. Also, from the same figure, we observed that Lin & Jiang model leads to better image resolution than that of Kalos model, which itself has better resolution image than Burke & Beck one. Such observation was clearly explained with vertical and horizontal image profiles shown in Figures 4 and 5.

Fig. 4. Vertical profiles of projected phantom image with (Lin & Jiang, Burke & Beck and Kalos) and without BUF considering

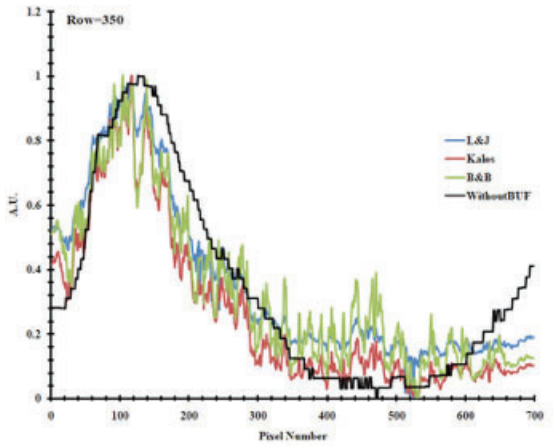

Fig. 5. Horizontal profiles of projected phantom image with (Lin & Jiang, Burke & Beck and Kalos) and without BUF considering

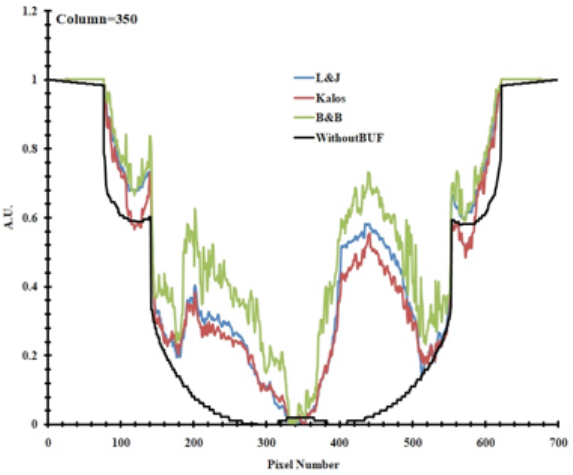

From profiles plotting, we see the close behave for L&J and Kalos models. Moreover, as horizontal profiles cross arms, lung and heart organs, they are configured with two peaks on the right side and three peaks on the left side. On the other hand, the BUF effect on imaging internal organs is well explained when comparing different models to the simple "WithoutBUF" model.

Tabulated statistical analysis of different images were given in Table 2, confirming the closeness of L&J and Kalos models. However, this study was limited to current setup of photon particle with 150 keV energy and can be extended to polychromatic exposure and to other kind of particles. Also, a straightforward application for radiotreatment purposes (Brachytherapy, Teletherapy) other than diagnosis, can be conducted allowing the large physicist community to advance knowledge on point-kernel ray-tracing technique for analysis of photon transport in a patient's body.

Table 2. Statistical image analysis for comparing the three studied models: signal-to-noise ratio (SNR), peak signal-to-noise ratio (PSNR), root mean square error (RMSE), mean average error (MAE) and structural similarity index (SSIM.)

Ref Image	Test Image	SNR	PSNR	RMSE	MAE	SSIM
L & J	B & B	19.095	22.136	13.215	11.026	0.940
L & J	Kalos	22.105	25.146	9.345	7.459	0.886
B & B	Kalos	16.243	19.687	19.696	17.305	0.879

4.Conclusion

An important parameter to quantify scattered beam contribution to the exposure is the buildup factor of a material for gamma-ray attenuation. Among the existing models describing BUF for multilayer shielding, we developed a C++ program able to choose between Lin & Jiang or Kalos or Burke & Beck ones. Such in-house program was able to produce the projected image of the thorax part of HDRK man irradiated with photon point source with energy 150 keV on a 700×700 mm2 detector. Hence, based on the developed computer code, a simple and flexible tool for computation of radiographic image is presented. Through the developed computer code, the influence of different multilayer BUF models on the image quality is investigated. Using this method requires little computational time on a single-processor PC compared to probabilistic methods. Moreover, we found that Lin & Jiang and Kalos models are statistically close to each other and the best resolution was seen for Lin & Jiang studied case. Despite this, we can conclude that the proposed results are important for medical imaging and radiation treatment planning for the vast majority of existing examination scenarios.

Conflict of Interest

The author declared no potential conflicts of interest with respect to the research, authorship, and/or publication of this article.

Acknowledgements

The author extend his appreciation to the College of Applied Medical Sciences Research Center and the Deanship of Scientific Research at King Saud University, Saudi Arabia.

References

[1]Ekelund L, Elzubeir M. Diagnostic radiology in an integrated curriculum: evaluation of student appraisal. Acad Radiol 2000; 7:965 –970

[2]Richard B. Gunderman1, Aslam R.

Siddiqui, Darel E. Heitkamp and Hal D. Kipfer. The Vital Role of Radiology in the Medical School Curriculum. American Journal of Roentgenology. 2003;180: 1239-1242

[3]C. Debus, U. Oelfke and S. Bartzsch, A point kernel algorithm for microbeam radiation therapy. Phys. Med. Biol. 62 (2017) 8341-8359.

[4]Th.I. Gotz, C. Schmidkonz, S. Chen, S. Al-Baddai, T. Kuwert et al., A deep learning approach to radiation dose estimation. Phys. in Med.& Bio. 65(3), 035007 (2020).

[5]A. Akhavanallaf, I. Shiri, H. Arabi, H. Zaidi, Whole-body voxel-based internal dosimetry using deep learning. Eur J Nucl Med Mol Imaging (2020).

[6]Y. Liang, W. Muhammad, G.R. Hart et al., A general-purpose Monte Carlo particle transport code based on inverse transform sampling for radiotherapy dose calculation. Sci Rep 10, 9808 (2020).

[7]L.G. Hanin, A stochastic model of tumor response to fractionated radiation: limit theorems and rate of convergence Math. Biosci. 191, 1-17 (2004).

[8]S.F.C. O'Rourke, H. McAneney and T. Hillen, Linear quadratic and tumour control probability modelling in external beam radiotherapy J. Math. Biol. 58 799-817 (2009).

[9]M. Zaider and L. Hanin, Tumor control probability in radiation treatment Med. Phys. 38 574-583 (2011).

[10]J. Gong, M.M. Dos Santos, C. Finlay and T. Hillen, Are more complicated tumour control probability models better? Math. Med. Biol. 30 1-19 (2013).

[11]A.V.P. Bobadilla, P.K. Maini and H. Byrne, A stochastic model for tumour control probability that accounts for repair from sublethal damage Math. Med. Biol. 35 181-202 (2018).

[12]W.R. Nelson, H. Hirayama and D. Rogers, The EGS4 code system, SLAC-265, Standford Linear Accelerator Center (1985).

[13]S. Agostinelli, J. Allison, K. Amako et al., Geant4-a simulation toolkit. NIMA 506(3), 250-303 (2003).

[14]O. Kadri, A. Alfuraih, Photon energy absorption and exposure buildup factors for deep penetration in human tissues. Nucl. Sci. Tech. 30, 176 (2019).

[15]K. Takeuchi, S. Tanaka, PALLAS-ID(VII), a code for direct integration of transport equation in one dimensional plane and spherical geometries. JAERI-M84, 214 (1984).

[16]D.V. Gopinath, K. Samthanam, Radiation transport in one dimensional finite technique. Nucl. Sci. Eng. 43 (2), 186 (1971).

[17]Y. Sakamoto, S. Tanaka, Y. Harima, Interpolation of gamma ray buildup factors for isotropic source with respect to atomic number. Nucl. Sci. Eng. 100 (1), 33-42 (1988).

[18]A. Shimizu, Calculations of gamma-ray buildup factors up to depths of 100 mfp by the method of invariant embedding, (I) analysis of accuracy and comparison with other data. J. Nucl. Sci. Technol. 39, 477-486 (2002).

[19]Eisenhauer, C.M., Simmons, G.L., Point isotropic gamma ray buildup factors

in concrete. Nucl. Sci. Eng., 56 (3) 263-270 (1975).

[20]C. Suteau, M. Chiron, An iterative method for calculating gamma ray buildup factors in multi-layer shields. Radiat. Prot. Dosim. 116 (1-4), 489-492 (2005).

[21]Y. Harima, Y. Sakamoto, S. Tanaka et al., Validity of the geometric progression formula in approximating gamma ray buildup factors. Nucl. Sci. Eng. 94, 24-35 (1986).

[22]M.H. Kalos, A Monte Carlo calculation of the transport of gamma rays, NDA 56-10 (1957).

[23]Burke G. de P. and Beck H. L., Calculated and measured dose buildup factors for gamma rays penetrating multilayered slabs. Nucl. Sci. Eng 53, 109-112 (1974).

[24]L. Uei-Tyng Lin, J. Shiang-Huei, A dedicated empirical formula for -ray buildup factors for a point isotropic source in stratified shields, Rad. Phys. and Chem. 48(4), 389-401 (1996).

[25] Duvauchelle, P., Freud, N., Kaftandjian, V., Babot, D., A Computer Code to Simulate X-Ray Imaging Techniques, Nucl. Instr. and Meth., B170 (2000), 1-2, pp.245-258.

[26] Gliere, A., SINDBAD: from CAD Model to Synthetic Radio graphs, in: Re view of Progress in Quantitative Non destructive Evaluation (Eds. D. O. Thomson, D. E. Chimenti), Vol. 17A, Plenum Publishing Co., Bristol and Philadelphia, USA, 1998

[27]Ljubenov, V., Simovi, R., Markovi, S., Ili, R. D., Photon Scattering and Reflection in Medical Diagnostic Energy Domain, Nuclear Technology & Radiation Protection, 23 (2008), 1, pp. 31-36

[28]Marinkovi, P., Ili, R. Spai, R., A 3-D Point-Kernel Multiple Scatter Model for Parallel-Beam SPECT Based on a Gamma-Ray Buildup Factor, Phys. In Med. and Biol. 52 (2007), 19, pp. 5785-5802,

[29]Kim, Chan Hyeong et al. "HDRK-Man: a whole-body voxel model based on high-resolution color slice images of a Korean adult male cadaver." Physics in medicine and biology 53 15 (2008): 4093-106 .

[30]Berger, M.J., Hubbell, J.H., Seltzer, S.M., Chang, J., Coursey, J.S., Sukumar, R., Zucker, D.S., and Olsen, K. (2010), XCOM: Photon Cross Section Database (version 1.5). [Online] Available: http://physics.nist.gov/xcom [2021, September 20]. National Institute of Standards and Technology, Gaithersburg, MD.

[31]Schindelin, J., Arganda-Carreras, I., Frise, E., Kaynig, V., Longair, M., Pietzsch, T., … Cardona, A. (2012). Fiji: an open-source platform for biological-image analysis. Nature Methods, 9(7), 676–682.

[32]D. Sage, M. Unser, Teaching Image-Processing Programming in Java, IEEE Signal Processing Magazine, vol. 20, no. 6, pp. 43-52, November 2003.

[33]Z. Wang, A. C. Bovik, H. R. Sheikh and E. P. Simoncelli, "Image quality assessment: From error visibility to structural similarity, " IEEE Transactions on Image Processing, vol. 13, no. 4, pp. 600-612, Apr. 2004.